9 Molecular Dynamics Simulation of Phospholipid Bilayers

Scott Feller

Department of Chemistry, Wabash College, 301 W. Wabash, Crawfordsville IN 47933, USA

E-mail: fellers@wabash.edu

Abstract. Molecular dynamics simulation of lipid bilayers is a rapidly developing field driven by the need to obtain an atomic-level picture of membrane structure and dynamics. As the discipline matures there will be many opportunities to extract information from simulation results that can be utilized in the interpretation and design of laboratory experiments. This chapter provides an overview of the molecular dynamics method and discusses some simulation results that may be of interest to experimentalists.

9.1 Overview of Molecular Dynamics Simulation

During the past decade advances in computational hardware and simulation methodologies have moved the field of molecular dynamics (MD) simulation at an incredible pace. There is no better example of this development than the MD simulation of lipid membranes. An early "membrane" simulation examined the behavior of water molecules, between surfaces composed of lipids molecules frozen in place, for a total of 8 picoseconds (ps) [1]. A pioneering work representing the membrane interior in atomic detail is the simulation of van der Ploeg and Berendsen where a decanoate bilayer (without solvent) was followed for 80 ps [2]. Today, bilayer simulations describing both lipid and solvent in full atomic detail are commonplace, with recent reports of trajectories of length 10 nanoseconds (ns) [3, 4]. While MD simulation in general has grown with advances in processing power, the lipid simulation field has especially benefited because membrane simulations typically include a large number of molecules in the system. Additionally, several algorithmic developments have increased the quality of lipid simulations. These include methods such as particle mesh Ewald (PME) summation [5] for the accurate calculation of Coulombic intermolecular forces between lipid headgroups and water, constant pressure ensembles that allow dynamic adjustment of membrane size and shape [6], and multiple time step algorithms that promise order of magnitude increases in simulation length [7].

During this period of growth and development of the lipid simulation field, exchange of information between experimentalists and simulators was largely unidirectional. Simulators took experimental data, such as the deuterium order parameter profile obtained from NMR [8] and the electron density profile from x-ray scattering [9], to assess the validity of the simulated structures. Dynamical infor-

mation, for example from NMR relaxation [10] and neutron scattering measurements [11], served as a test of the time scales observed in the simulation. More recently the exchange of data has begun to occur in both directions and, although the rates of exchange may yet be unequal, it is clear that the potential for collaboration between experimentalists and simulators is great.

In the remainder of this section, a brief overview of the molecular dynamics method will be presented with an emphasis on those aspects most relevant for the simulation of fluid phase lipid bilayers. For a more thorough discussion of MD simulation in the reader is referred to reference [12] (for a general description) or [13] which focuses on biomolecular simulation. Reviews covering membrane simulation specifically include the articles by Pastor [14], Tobias, et al. [15], Jakobsson [16], and Berendsen [17]. In sections 9.2, an example of the use of simulation in the refinement of experimental data from diffraction studies is reviewed [18].

9.1.1 Potential Energy Functions

The energy function, U, is central to the method of molecular dynamics simulation. All interactions, both intramolecular and intermolecular must be faithfully represented by an empirical function of the atomic coordinates. In principle U may take on any form, however, as a practical matter it should be differentiable (to analytically determine forces) and must contain a sufficient number of parameters to accurately describe the potential energy surface without having more parameters than can be reasonably estimated. Popular programs for biomolecular simulation such as CHARMM [19], AMBER [20], and GROMOS [21] typically contain intramolecular terms for bond lengths, bond angles, and torsion angles, and intermolecular terms representing Coulombic and dispersion interactions. In the following a brief description of the energy function used within CHARMM is given, the format of the specific force field employed in a simulation is usually given (or should be given) within the methods sections of an article. For a more complete description of phospholipid parameter set development, the reader is referred to reference [22].

The bond energy is represented by a harmonic function of the difference between instantaneous and equilibrium bond length

$$U(l) = \sum_{bonds} k_b (l - l_0)^2 \qquad (9.1)$$

Notice that in CHARMM a nonstandard definition of the force constant is used to eliminate multiplications, such subtle differences often make direct comparison of force-field parameters difficult. Values for l_0 and k_b are typically fit to reproduce equilibrium geometries and vibrational frequencies of simple model compounds. For example, parameters for the alkyl chains in the lipid bilayer might be determined by fitting the parameters to the experimental geometry and frequencies for butane. From an MD simulation one can calculate the potential of mean force, $W(l) = -kT \ln[P(l)]$, where $P(l)$ is the probability distribution for bond lengths. The potential of mean force (a product of the simulation) can be compared with

the potential energy function (input to the simulation) to determine the effect of neighboring atoms on the bond length distribution. This quantity has been calculated for the both length of carbons at the center of the fatty acid chains of DPPC and in Figure 1 is compared it to the "bare potential" U(*l*) that was used in the simulation. Figure 1 shows (not surprisingly) that the shape of the potential energy function largely determines the bond length distribution. In other words, the bond length takes on approximately the same values expected of an isolated harmonic oscillator with these potential energy parameters.

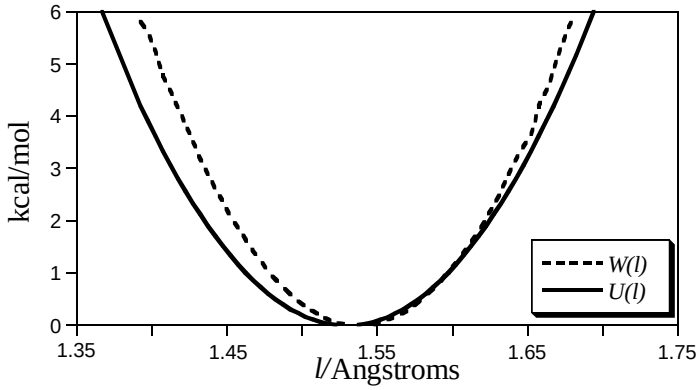

Fig. 9.1. Potential of mean force, W (dashed), and bare potential, U (solid), for the length of the C7-C8 bond.

The bond angle energy, also typically represented by a quadratic function, depends on the difference between the instantaneous and equilibrium values of the bond angle.

$$U(\theta) = \sum_{angles} k_\theta (\theta - \theta_0)^2 \tag{9.2}$$

As with the bond length, parameters for the bond angles are fit to reproduce equilibrium geometries and vibrational frequencies. Within the CHARMM potential energy function an additional function, the Urey-Bradley term,

$$U(r^{1-3}) = \sum_{angles} k_{1-3} (r^{1-3} - r_0^{1-3})^2 \tag{9.3}$$

is included to obtain a satisfactory description of the vibrational modes. This contribution is a quadratic function of the distance between atoms separated by two chemical bonds; thus it depends on the two bond lengths and the bond angle between the atoms. Calculation of the C7-C8-C9 bond angle shows that, as with the bond length, the potential of mean force is largely determined by the bare potential. The difference between W and U is also similar for bond lengths and

bond angles, in both cases the neighboring atoms tend to restrict the motion of the atoms compared to the values predicted for the isolated oscillators.

One of the most critical components of the potential energy function for chain molecules such as lipids is the torsional potential. Early simulations of butane [23] used a two term Fourier series in the dihedral angle, ϕ

$$U(\phi) = \sum_{dihedrals} k_\phi \left[\cos\left(n\phi - \phi_0\right) + 1\right] \tag{9.4}$$

Two terms, one with n=1 and a second with n=3 (both with ϕ_0=0), are sufficient to produce a torsional potential energy surface, typical of alkanes, with two local minima corresponding to the *gauche* conformations and a global minimum at the *trans* position. Appropriate choices of ϕ_0 and n can similarly produce energy surfaces for rotation around double bonds, however, the barriers to rotation are typically too large to be sampled in an MD simulation making energy differences between conformers less important. In addition to the bare torsional potential (Eq. 9.4) the potential energy surface is also influenced by Coulombic and dispersion interactions between atoms separated by three or more chemical bonds. These "1-4" interactions are omitted or scaled from their full strength in many parameters sets but are not modified in the CHARMM lipid parameter set [22]. The dihedral parameters are generally fit to reproduce conformational energy differences, e.g. between gauche and trans, and rotational barrier heights. These energies are obtained from a combination of experimental data and ab initio quantum mechanical calculations. Figure 9.2 gives the potential of mean force for rotation about the central dihedral of the palmitic acid chain of DPPC using the current CHARMM potential function. This parameterization includes 4 cosine terms fit to high level ab initio results [24]. The bare torsional potential (Eq. 9.4) is included in figure 9.2 for comparison along with the complete butane potential energy surface. From the figure it is clear that the 1-4 interactions contribute significantly to the potential energy surface and that parameterizations that neglect these interactions will, by necessity, employ a very different bare torsional potential energy function. From the butane energy surface the difference between trans and *gauche* states is 0.63 kcal/mol, and from the DPPC distribution a gauche fraction of 23% is obtained. Both are in good agreement with experimental estimates from IR spectroscopy [25, 26].

The remaining terms in the potential energy function describe inter-molecular forces. The dispersion or van der Waals interaction is modeled using the Lennard-Jones 6-12 potential

$$U = \sum_i \sum_{j<i} \varepsilon_{ij} \left[\left(\frac{\sigma_{ij}}{r_{ij}} \right)^{12} - \left(\frac{\sigma_{ij}}{r_{ij}} \right)^{6} \right] \tag{9.5}$$

where ε is a measure of the attraction between atoms and σ is determined by the sizes of the atoms. The double summation in Eq. 9.5 is formally over all intermolecular pairs and over all intramolecular pairs separated by more than two chemical bonds. In practice, however, the summation is truncated so as to include only atom pairs separated by a distance less than the cutoff radius, r_c. The short-range nature (r^{-6}) of these interactions allows cutoff radii in the range of 8-14 Å to

be employed with relatively small errors introduced into the forces. To further reduce these errors termination functions are often used that smoothly bring the interaction to zero over the outermost 1-2 Å of the cutoff sphere, removing discontinuities in the potential. Energies and pressures can be corrected for the neglect of long-range van der Waals attraction [12] using a continuum approximation for the region outside r_c, however, these are rarely applied in membrane simulations because the anisotropic structure makes the use of these methods awkward. Lennard-Jones interactions are typically refined by carrying out condensed phase simulations and adjusting the parameters to reproduce experimental densities and heats of vaporization. Many lipid parameter sets have used experimental data from crystal structures of lipids (or lipid fragments) in developing these parameters, as well as liquid state properties of neat alkanes [27].

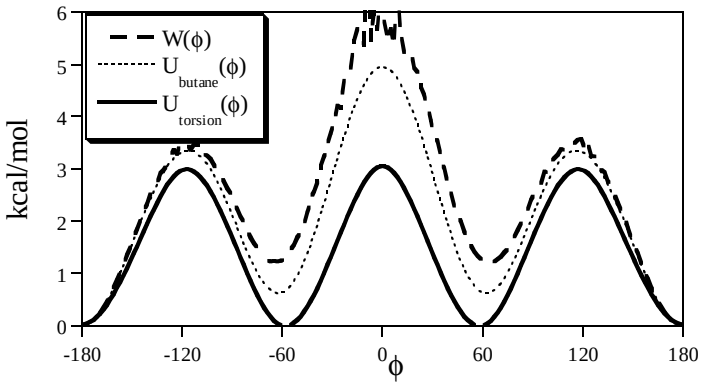

Fig. 9.2. Potential of mean force, W (long-dash), and bare potential, U (solid), for the C7-C8-C9-C10 dihedral angle. The short dashed line gives the potential energy surface for butane.

The final term in the CHARMM energy function accounts for Coulombic interactions between non-bonded atoms,

$$U = \sum_i \sum_{j<i} \frac{q_i q_j}{r_{ij}} \tag{9.6}$$

Where q is the partial charge assigned to each atom. This term is crucial for a successful description of lipid bilayer structure because of the strong headgroup-headgroup, headgroup-solvent, and solvent-solvent interactions, all of which contain a large electrostatic component. Assignment of atomic partial charges is often based on ab initio calculations, however, some groups have found it necessary to scale the charges up [28] or down [29] to obtain stable bilayer simulations. In addition to experimental dipole moments and aqueous heats of solvation, the CHARMM force field charges are also determined by ab initio calculations, but in a very different manner. Complexes formed from small model compounds, e.g. tetramethylammonium, and water were studied quantum mechanically to determine the intermolecular potential energy surface. The charges were subsequently

adjusted to fit the empirical energy surface to the quantum mechanical result. This approach emphasizes the importance of lipid-solvent interactions in the parameterization. Simulations of the alkane/water interface tested the hydrophobic interaction between water and the hydrocarbon core of the membrane. These simulations allow direct evaluation of the surface tension and provide an especially sensitive test of inter-molecular potentials. Simulations of water/octane and water/1-octene using the CHARMM force field produced surface tensions in good agreement with experiment and were able to reproduce the surface tension lowering due to unsaturation [30].

The evaluation of Coulombic interactions is an important methodological issue in membrane simulation. In the periodically replicated simulation cell generally used for bilayer simulations, the double summation in Eq. 9.6 formally includes all atoms and their periodic images (an infinite sum). In contrast to the Lennard-Jones potential with its rapid r^{-6} convergence, truncation of the r^{-1} electrostatic potential can lead to severe artifacts in an MD simulation. The most common effect is increased structure induced by force truncation, e.g. the decay length for orientational ordering of water at the DPPC membrane interface increased 50% when spherical truncation at r_c = 12 Å was used [31]. Many techniques have been developed to minimize the errors using termination functions [32], while others have employed algorithms that modify the interaction pair list. For example, the intermolecular interactions can be evaluated based on distance between molecules, rather than atoms, to insure that forces are calculated between electrically neutral groups. Membrane simulations have also been designed such that hydrocarbon-hydrocarbon interactions are truncated at relatively short distances (~9 Å) while headgroup-water interactions were calculated over a much longer range (20 Å). The most reliable approach, however, appears to be the use of Ewald summation techniques. The Ewald method breaks the summation in Eq. 9.6 down into two summations, a short ranged term that is summed in real space to r_c ~10 Å and a second term that is calculated in reciprocal space (taking advantage of the periodic nature of the system). The high accuracy of the Ewald summation comes with a large computational expense that scales approximately as N^2 (making it costly for large systems such as hydrated bilayer membranes). An improved algorithm, the Particle Mesh Ewald (PME) method [5], relies on fast Fourier transform methods to determine the reciprocal space summation and is sufficiently fast for use in bilayer simulations.

9.1.2 Equations of Motion

The most conceptually simple algorithm for molecular dynamics simulation maintains constant particle number (N), volume (V), and energy (E), and involves numerical solution of the Newtonian equations of motion for each atom in the system

$$\ddot{x} = F_x / m \qquad F_x = -\left(\frac{\partial U}{\partial x}\right) \tag{9.7}$$

where m and F_x are the mass and x component of force, respectively. Equivalent expressions for y and z are also included for each of the N atoms. Starting from an initial set of coordinates and velocities, the forces on each atom are calculated from the derivatives of the potential energy function described in section 9.1.1. Equation 9.7 cannot be solved analytically but is relatively simple to solve numerically (at least as compared to typical coupled and nonlinear differential equations encountered in physics and chemistry). A particularly simple algorithm for solving the equations of motion is the Verlet algorithm [33]

$$x(t+\Delta t) = 2x(t) - x(t-\Delta t) + \frac{F_x(t)}{m}\Delta t^2 \tag{9.8}$$

which gives the position of each atom based on the current position and force along with the previous position. The Verlet algorithm is derived from Taylor's series expansions about *x(t)*

$$x(t+\Delta t) = x(t) + \dot{x}(t)\Delta t + \tfrac{1}{2}\ddot{x}(t)\Delta t^2 \tag{9.9}$$

$$x(t-\Delta t) = x(t) - \dot{x}(t)\Delta t + \tfrac{1}{2}\ddot{x}(t)\Delta t^2 \tag{9.10}$$

adding Eqs. 9.9 and 9.10 substituting Eq. 9.7 for the acceleration gives the Verlet equation for position. Notice that the velocities $(v_x(t) = \dot{x}(t))$ are not needed to calculate the trajectory. They are used, however, for the calculation of kinetic energy and pressure and can be determined within the Verlet scheme by subtracting Eq. 9.9 from 9.10

$$v_x(t) = \frac{x(t+\Delta t) - x(t-\Delta t)}{2\Delta t} \tag{9.11}$$

There are several variations on the basic Verlet algorithm; examples are "leap-frog Verlet" and "velocity Verlet". All generate identical trajectories in the microcanonical (NVE) ensemble, but differ in the definition of the velocities. The definition of velocity becomes important when implementing algorithms for molecular dynamics in the canonical (NVT) or isothermal-isobaric (NPT) ensembles. These methods, which have recently gained widespread use in the simulation of bilayer systems, modify the equations of motion given by Eq. (9.7) to maintain the temperature and/or pressure at a fixed value. Many groups have adopted the "extended system" formalism, originally due to Andersen [34], for constant pressure MD. An additional degree of freedom is added to the simulation, corresponding to the volume of the cell, with the force acting on this added degree of freedom determined by the difference between instantaneous and applied (target) pressures. For a cubic simulation cell, the equations of motion become

$$\dot{x} = v + \tfrac{1}{3}\frac{\dot{V}}{V}x \qquad \dot{v}_x = \frac{F_x}{m} - \tfrac{1}{3}\frac{\dot{V}}{V}v_x \qquad V = \frac{1}{W}\left[P(t) - P_{ext}\right] \tag{9.12}$$

where W is the "mass" parameter for the extra degree of freedom (this degree of freedom is often referred to as the piston). The value of the mass does not influence equilibrium properties but does affect the rate at which the system responds

to the pressure imbalance. As a practical mater the mass must be sufficiently small that the system can respond on the MD time scale, however, very small masses may lead to unphysical oscillations with frequency proportional to $W^{-½}$. Extensions to Andersen's method have been described allowing the use of noncubic simulation cells [35], the addition of a constant temperature degree of freedom [36], and the control of oscillations by means of a Langevin equation [37].

The application of constant pressure MD to lipid bilayers is complicated by the anisotropic nature of the system. In contrast to a simulation of pure water or a neat alkane where only the size of the cell need vary, the dimension in the directions lateral and normal to the membrane must change independently due to the large differences in compressibility. Additionally, it is unclear what the value of the applied pressure tensor should be for patch of membrane having nanometer dimension as there are no experiments probing this quantity [38]. The difference between lateral and normal components of the pressure tensor is proportional to the surface tension, γ, at the interface [6]. Arguments have been given for a range of γ values that should be used in bilayer simulation. From considering macroscopic membrane thermodynamics, it has been suggested that bilayer surface tension must be zero because the system is at its free energy minimum with respect to surface area [39, 40]. Others have argued that the surface tension of monolayer films at corresponding surface areas should be used [41], however this approach is complicated by the existence of the fatty acid/air interface. Additional factors, related to the confining effect that periodic boundary conditions have on membrane dynamics, were ignored in these analyses and recent calculations [42-44] have shown that an additional nonzero surface tension is required when carrying out simulations of small systems.

9.1.3 Summary

In concluding this outline of the molecular dynamics method we wish to emphasize that there are many issues to be considered when planning an MD simulation (or when evaluating the validity of simulation results). Several have been discussed here: potential energy function and its parameterization, numerical integration method and length of time step, treatment of long-range electrostatic forces, and choice of statistical mechanical ensemble. An ever present concern is the length of the simulation [45], e.g. were the properties of interest sufficiently sampled that the results are statistically significant? Another issue is the size of the simulation cell. To date the number of molecules included in the simulation has been determined by hardware limitations and has been in the range of 10,000-20,000 atoms, however, further research may show that the small length scales inherent in these simulations are not sufficient for some problems.

Many of these issues will become even more critical as simulations of complex model membranes are attempted. For example, simulations of pure lipid membranes benefit from the increased precision available by averaging over the properties of many (50-100) indistinguishable molecules. A simulation of a single ion channel in a membrane, however, may need to be followed for a length 50-100 times greater to obtain equivalent statistics. Additionally, systems with low solute/lipid ratios may require many lipid molecules to faithfully reproduce the mac-

roscopic conditions. The recent history of hardware and algorithmic advances, along with the rapid growth of parallel computing, suggest these problems will be addressed early in the coming decade.

9.2 Determination of Lipid Component Volumes

Subtle experimental techniques are available to determine the molecular volumes of phospholipids, with a precision of a few $Å^3$ [46-48]. In the next subsection the determination of the volume of arbitrarily defined *fragments* of the phospholipid molecule from molecular dynamics simulations is described. The application of this method to saturated and unsaturated phosphatidylcholines is demonstrated in 9.2.2, and in 9.2.3 we show how this data may be used in "liquid crystallography" methods for the interpretation of x-ray and neutron diffraction experiments.

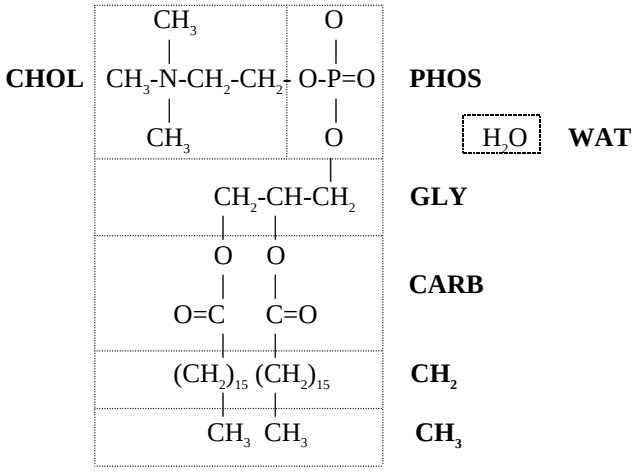

Fig. 9.3. Definition of molecular fragments used in the present analysis.

9.2.1 Method of Calculation

We describe briefly here the algorithm used to extract information on the volume of lipid fragments from an MD simulation, for a more thorough discussion the reader is referred to references [18, 48]. The lipid molecule is first parsed into arbitrarily defined fragments. Figure 9.3 gives the fragment definitions for DPPC used here. This particular partitioning scheme is motivated by the fragment definitions of Wiener and White in their series of papers describing the structure of a dioleoylphosphtidylcholine (DOPC) bilayer [49, and references therein]. Next, the time-averaged transbilayer distribution of the fragments is obtained from the MD

simulation trajectory. This distribution is plotted in figure 9.4 for fluid phase DPPC. The central idea behind the method is that slabs of equal cross sectional area A and equal thickness Δz must have identical slab volume, V_s, equal to $A \times \Delta z$. This slab volume must be filled by the sum of the volumes occupied by each fragment.

$$V_s = \sum_{i=1}^{\#\ of\ components} n_i(z) \times V_i \tag{9.13}$$

This equation must be satisfied for each of the slabs in the simulation cell, thus Eq. 9.13 is actually a set of coupled linear equations (the unknowns are the $\{V_i\}$). Dividing the simulation cell into a large number of slabs insures that the solution is overdetermined and the optimal set of V_i is found by minimizing

$$F = \sum_{j=1}^{\#\ of\ slabs} \left(V_s - \sum_{i=1}^{\#\ of\ components} n_i(z_j) \times V_i \right)^2 \tag{9.14}$$

The principal assumption within this method is that the volumes are independent of location within the membrane, e.g., the volume of methylenes near the headgroup is equal to the volume near the bilayer center and the volume of water molecules hydrating the headgroups are the same as bulk water. In principle, MD simulations should be able to test this assumption and work continues in this laboratory in that area. To date, we have carried out volume fits that included only certain regions of the DPPC simulation cell, but were unable to find statistically significant changes in water or methylene volume. Longer simulations, however, may be able to detect small changes in component volumes.

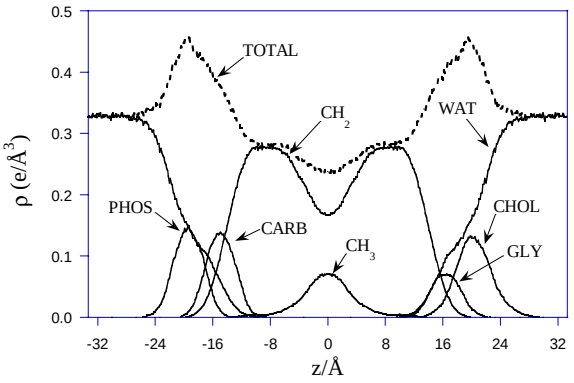

Fig. 9.4. Electron density as a function of position along the bilayer normal. The $n_i(z)$ were obtained from the electron density due to each group by the number of electrons per group.

9.2.2 Phosphatidylcholine Fragment Volumes

We have used the method outlined above to calculate fragment volumes from bilayer simulations of fully hydrated DPPC [50] and DOPC at low hydration [30]. Both simulations were broken into 100 ps blocks, the time-averaged density profiles obtained for each block, and the optimal fragment volumes determined from minimization of equation 9.14. Table 9.1 lists the average component volumes from each simulation.

The small, but statistically significant differences, between DPPC and DOPC methyl and water fragments can be attributed to the ~25°C temperature difference between the simulations (simulations of bulk water and hexadecane carried out over this temperature range confirmed the observed temperature dependence). Additional statistically significant differences were found for headgroup volumes, but this discrepancy may be an artifact of the fitting procedure caused by some pairs of groups lying mostly parallel to the plane of the membrane, e.g. phosphate and choline. If the density of the two groups is located largely in the same region along z, the volume of the slab can be assigned to either group giving essentially the same quality fit. Both combinations, $V_{PHOS} + V_{CHOL}$ and $V_{GLY} + 2V_{CARB}$, were computed from each simulation and in these quantities no statistically significant differences were observed. This demonstrates, however, that individual headgroup fragments volumes are the least well resolved quantity in the present analysis. In order to obtain headgroup volumes with greater confidence, additional simulations differing in their fatty acid composition and hydration level were also analyzed. Average component volumes from all simulations are given in the last line of Table 9.1.

The set of average component volumes obtained from simulation can be compared against experimental data for molecular volume and headgroup volume. Adding component volumes for DPPC and DOPC gives 1212 and 1302 $Å^3$, in excellent agreement with their respective experimental values of 1232 [46] and 1295 [48]. The headgroup volume calculated from the simulation data is 321 $Å^3$, also in excellent agreement with experimental estimates of 319 [51] and 325 $Å^3$ [52].

Table 9.1. Volumes of lipid fragments. All values are given in $Å^3$. The average values are taken from reference [18] and include simulations of other lipids and other hydration levels.

	CH_3	CH_2	C=C	CARB	GLY	PHOS	CHOL	H_2O
DPPC	53.6	28.0	N/A	44.1	63.6	65.6	108.6	30.4
DOPC	52.8	28.1	45.9	37.4	81.6	51.1	129.7	29.5
Ave.	52.7	28.1	45.0	39.0	68.8	53.7	120.4	30.3

9.2.3 Interpretation of Diffraction Data

We have used the component volumes derived here to extend the “liquid crystallography” methods developed by Wiener and White [49] for structure determina-

tion of fluid bilayers. They have used the average transbilayer distribution of molecular fragments to describe the structure of a DOPC bilayer using a combination of x-ray and neutron diffraction data. These diffraction studies used a joint-refinement procedure that obtains a best fit for the positions (Z_i) and widths (A_i) of Gaussian distributions representing the location of molecular fragments along the bilayer normal. These structural parameters are fit simultaneously to the x-ray and neutron scattering data to minimize the joint crystallographic R-factor

$$R = \sum_{\substack{j=xray\\neutron}} R_j \tag{9.15}$$

$$R_j = \frac{\sum_h \left\| F_j(h) \right| - \left| F_j^*(h) \right\|}{\sum_h \left| F_j^*(h) \right|} \tag{9.16}$$

where the F_j are the structure factors (* denotes the experimental values) and h is the diffraction order.

The Gaussian distribution functions describing the bilayer structure give number density distributions similar to that obtained from the MD simulation, the difference being that no functional form is assumed in MD. Given a set of fragment volumes such as we have obtained from simulation and a number density distribution from diffraction refinement, it is straightforward to calculate the volume of fragments occupying arbitrarily defined slabs along the bilayer normal. In principle, each slab should have the identical volume (the product of the cross-sectional area and the slab thickness). We used this principle to include a constraint in the joint-refinement procedure of Wiener and White by adding a third term

$$R_{volume} = \left\langle \left(\frac{V_s - \sum_i n_i V_i}{V_s} \right) \right\rangle \tag{9.17}$$

where V_s is the slab volume, V_i is the fragment volume, the n_i are determined from the Gaussian distributions being refined, and the brackets denote an averaging over all slabs.

The number of structural parameters (Z_i and A_i's) determined in the joint-refinement is limited by the number of observed diffraction orders. At low hydration, Wiener and White were able to observe 8 orders from both x-ray and neutron diffraction. At full hydration it is difficult to obtain more than approximately 4 orders because of thermal fluctuations [9], making their method inapplicable to the study of the fully hydrated systems considered more representative of biological membranes. The addition of volumetric information has the effect of increasing the number of "experimental" data points and allows improved accuracy in the structure determination, in addition it allows solutions where fewer diffraction orders are observed as in the case of the more fully hydrated membrane systems.

In their joint-refinement of the structure of DOPC, Wiener and White kept the distribution of CH_3, C=C, and H_2O groups fixed at values they determined inde-

pendently in separate experiments. The positions and widths of the Gaussians representing carbonyl, glycerol, phosphate, and choline groups were free parameters as well as the number (N_i), position, and width of three distributions representing the methylene groups, for a total of 17 parameters. Using the relation that the sum of the methylene N_i must be 28, the number of parameters is reduced to 16. Combining their diffraction data with the present volumetric constraints, we have carried out structure refinements for DOPC using the diffraction data of Wiener and White and the average fragment volumes given in Table 9.1. The parameter values obtained are presented in Table 9.2 along with a set of their original results for comparison. The results presented here are based on the fits that converged to lower R values than each of the "self-R" values that measure the uncertainty in the experimental data [49]. The results from the two different procedures are in excellent agreement. Surprisingly, although the present method includes additional restraints, better fit to the x-ray and neutron data was obtained than in the original work. Additionally, the fraction of refinements that were successful increased upon addition of the volume restraint.

As mentioned previously, the number of available data points fixes the number of structural parameters that can be determined in the refinement. In addition to minimizing the difference between the 16 calculated and measured structure factors, 8 additional pieces of data have been included via the fragment volumes used to calculate R_{volume}. These additional data allow more complex models of the lipid bilayer to be investigated, e.g., by allowing fragments with positions fixed in the analysis of Wiener and White to vary as additional parameters. For the terminal methyl we investigated one and two Gaussian representations, having complete freedom in both Z and A, and found there was no significant improvement from the two function model. Every refinement trial using two Gaussians ended with both methyl groups (representing the individual monolayers) at the same positionin the center of the membrane. The water density was represented by two Gaussian

Table 9.2. Joint refinement results for the structure of DOPC. Positions (Z) and halfwidths (A) are given in units of Å. The number of methylenes represented by each Gaussian (N) are related by $N_1 + N_2 + N_3 = 28$. Asterisks denotes parameters that were fixed during the refinement procedure (their values were determined independently by specific labeling studies). P is the number of free parameters in the model.

	16 P			ref [49]			20 P		
Group	Z	A	N	Z	A	N	Z	A	N
CH_3	0.00*	2.95*		0.00*	2.95*		0.00	3.00	
CH_2(1)	3.70	1.61	1.04	2.95	2.84	3.67	3.69	1.62	0.99
CH_2(2)	6.29	5.44	13.49	6.09	3.88	7.18	6.38	5.33	14.19
CH_2(3)	13.57	4.71	13.47	12.76	5.19	17.15	13.66	4.61	12.82
C=C	7.88*	4.29*		7.88*	4.29*		8.35	4.52	
CARB	15.94	2.72		15.99	2.77		15.99	2.71	
GLY	18.82	2.27		18.67	2.46		18.89	2.25	
PHOS	20.13	3.09		20.15	3.09		20.16	3.04	
CHOL	21.98	3.45		21.86	3.48		21.88	3.55	
H_2O	22.51*	4.63*		22.51*	4.63*		24.55	5.49	

$R_{X\text{-}ray}$		0.012			0.022			0.013	
$R_{Neutron}$		0.051			0.062			0.042	
R_{Volume}		0.047			N/A			0.046	

distributions fixed at Z=±22.51 Å in the joint refinement of Wiener and White. After allowing both the position and halfwidth of the water distribution to be free parameters, we again compared two Gaussian representations against single functions centered at Z=d/2 (where d = the length of the unit cell). While both water distributions stayed near their respective initial conditions, the remaining fragment distributions moved from the initial conditions and under both protocols converged to similar final results. As the R_{total} obtained with a single water function centered at d/2 was lower than that obtained with a two Gaussian representation, and because the single distribution requires the determination of one less parameter, we adopted a single Gaussian representation for subsequent modeling.

The additional degrees of freedom available in the refinement can also be used to increase the number of Gaussian functions representing the methylene density. Our tests showed no advantage upon addition of a fourth Gaussian to describe the methylene region with the present data set; thus we employed the 3 Gaussian model proposed by Wiener and White for all subsequent analysis. It should be noted that in testing various representations for the methylene density, models using only two Gaussians obtained nearly the same levels of R as the three and four Gaussian representations. This suggests it may be possible to determine the structure of membranes where less experimental data is available by simplifying the methylene representation.

After examining a number of models to describe the transbilayer distribution of molecular fragments, we chose a 20 parameter model that assumes the methyl density to be centered around z=0, the water density to be centered around d/2, and the methylene density to be represented by the sum of 3 Gaussian distributions. The resulting structure is shown graphically in Figure 9.5 (parameter values are listed in the rightmost columns of Table 9.2) along with the original results of Wiener and White. Values obtained via refinement for the methyl and C=C widths are in good agreement with those assumed by Wiener and White (which were fixed rather than free parameters), although the C=C position is found 0.47 Å closer to the headgroup in the present analysis. The double bond, with its reduced number of hydrogens, scatters neutrons more strongly than methylene segments and the experimentally determined neutron scattering density has a small peak at ~8.3 Å, consistent with the present determination of $Z_{C=C}$ = 8.35 Å. The fit of the model to the x-ray and neutron diffraction results is as good or better with volumetric data even though this technique imposes additional constraints on the fitting procedure(some of the improvement, however, may be from the increased flexibility allowed by a 20 parameter model). A notable result from the present refinement is that 84% of the refinements were successful (the remainder did not meet the $R_{neutron}$ criteria), compared with an ~10% success rate reported by Wiener and White and the ~50% we observed in our first trials. The most significant difference between the structures depicted in Figure 9.5 is the location of the double bond, but this discrepancy is still less than 1 Å and, as mentioned previously, is supported by the small peak in the neutron scattering profile at ~8.3 Å.

While in the present work we have used equal weights for the x-ray, neutron, and volume data, this should ultimately be determined by an analysis of the esti-

mated relative error in the three data sets. The existence of the volume data also allows refinements of the original 16 parameter model of Wiener and White by combining the volumetric data with the x-ray and neutron data sets individually.

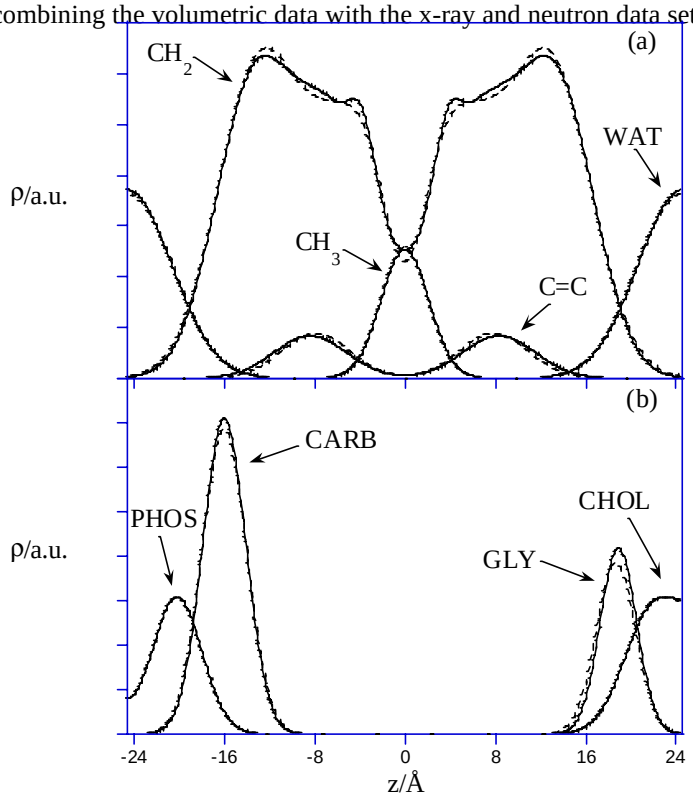

Fig. 9.5. Structure of DOPC. The dashed lines show the results of Wiener and White based on their diffraction data, and the solid lines display the present results using a combination of diffraction and volumetric data.

An interesting observation from these calculations is that the neutron data seem much more compatible with the volumetric information than the x-ray data, with the neutron+volume calculation obtaining an R_{volume} value that is less than 1/5 that of the x-ray+volume refinement.

9.3 Summary

As outlined in the present review, the synthesis of information obtained from laboratory experiments and computational studies has tremendous potential in the study of bilayer membranes. By application of atomic-level molecular dynamics simulations the volumes of submolecular lipid fragments and its position within

the lipid bilayer were obtained directly, where in the past, volume and positional estimates at this level of detail came only indirectly from interpretation of experimental data.
The method improved the accuracy in the structure determination and offers the ability to allow also the structural refinement of fully hydrated membrane systems, not applicable with current experimental data. In addition longer simulations offer the opportunity to reduce the error bars associated with the present results.

Acknowledgements. This work was supported by the National Science Foundation through grant MCB9728206.

References

9.1 R. Kjellander, S. Marchja: Perturbation of hydrogen bonding in water near polar surfaces, Chem. Phys. Lett. **120**, 393-396 (1985).
9.2 P. van der Ploeg, H.J.C. Berendsen: Molecular dynamics simulation of a bilayer membrane, J. Chem. Phys. **76**, 3271-3276 (1982).
9.3 U. Essmann, M.L. Berkowitz: Dynamical properties of phopholipid bilayers from computer simulation, Biophys. J. **76**, 2081-2089 (1999).
9.4 S.E. Feller, D. Huster, K. Gawrisch: Interpretation of NOESY cross-relaxation rates from molecular dynamics simulation of a lipid bilayer, submitted.
9.5 U. Essmann, L. Perera, M.L. Berkowitz, T. Darden, H. Lee, L.G. Pedersen: A smooth partical mesh Ewald method, J. Chem. Phys. **103**, 8577-8593 (1995).
9.6 Y. Zhang, S.E. Feller, B.R. Brooks, R.W. Pastor: Computer simulation of liquid/liquid interfaces. I. Theory and application to octane/water, J. Chem. Phys. **103**, 10252-10266 (1995).
9.7 M. Watanabe, M. Karplus: Dynamics of molecules with internal degrees of freedom by multiple time-step methods, J. Chem. Phys. **99**, 8063-8074 (1993).
9.8 A. Seelig, J. Seelig: Insert title here, Biochemistry **13**, 4839-4845 (1974).
9.9 J.F. Nagle, R. Zhang, S. Tristram-Nagle, W. Sun, H. Petrache, and R.M. Suter: X-ray structure determination of fully hydrated L_α phase dipalmitoylphosphatidylcholine bilayers, Biophys. J. **70**, 1419-1431 (1996).
9.10 M.F. Brown: Membrane structure and dynamics studied with NMR spectroscopy, in *Biological membranes: A molecular perspective from computation and experiment*, ed. By K.M. Merz & B. Roux (Birkhauser, Boston 1996) pp. 175-254.
9.11 W.L.C. Vaz, P.F. Almeida: Microscopic versus macroscopic diffusion in one-component fluid phase bilayer membranes, Biophys. J. **60**, 1553-1554 (1991).
9.12 M.P. Allen, D.J. Tildesley: *Computer simulation of liquids* (Clarendon, Oxford 1987).
9.13 W.F. van Gunsteren, P.K. Weiner, A.K. Wilkinson: *Computer simulation of biomolecular systems: Theoretical and experimental applications* (ESCOM Science Publishers, Leiden 1993).
9.14 R.W. Pastor: Molecular dynamics and Monte Carlo simulations of lipid bilayers, Curr. Opin. Struct. Biol. **4**, 486-492 (1994).
9.15 D.J. Tobias, K. Tu, M.L. Klein: Atomic-scale molecular dynamics simulations of lipid membranes, Curr. Opin. Colloid and Interface Sci. **2**, 115 (1997).

9.16 E. Jakobsson: Computer simulation studies of biological membranes: progress, promise and pitfalls, Trends in Biological Science **22**, 339-344 (1997).

9.17 H.J.C. Berendsen, D.P. Tieleman: Molecular dynamics: studies of lipid bilayers, in *Encylopedia of Computational Chemistry* (Wiley, 1998).

9.18 R.S. Armen, O.D. Uitto, S.E. Feller: Phospholipid component volumes: Determination and application to bilayer structure calculations, Biophys. J. **75**, 734-744 (1998).

9.19 B.R. Brooks, R.E. Bruccoleri, B.D. Olafson, D.J. States, S. Swaminathan, and M. Karplus: CHARMM: A program for macromolecular energy, minimization, and dynamics calculations, J. Comp. Chem. **4**,187-217 (1983).

9.20 D.A. Pearlman, D.A. Case, J.C. Caldwell, G.L. Seibel, U.C. Singh, P. Weiner, P.A. Kollman: *AMBER 4.0* (University of California, 1991).

9.21 W.F. van Gunsteren, H.J.C Berendsen: *Groningen Molecular Simulation (GROMOS) library manual* (Biomos, Groningen 1987).

9.22 M. Schlenkrich, J. Brickman, A.D. MacKerell, Jr., M. Karplus: An empirical potential energy function for phospholipids: Criteria for parameter optimization and applications, in *Biological membranes: A molecular perspective from computation and experiment*, ed. By K.M. Merz & B. Roux (Birkhauser, Boston 1996) pp. 31-82.

9.23 J.P. Ryckaert, A. Bellemans: Molecular dynamics of liquid *n*-butane near its boiling point, Chem. Phys. Lett. **30**, 123-125 (1975).

9.24 G.D. Smith, R.L. Jaffe: Quantum chemistry study of conformational energies and rotational energy barriers in n-alkanes, J. Phys. Chem. **100**, 18718-18724 (1996).

9.25 S Kint, J.R. Scherer, R.G. Snyder: Raman spectra of liquid n-alkanes. III. Energy difference between trans and gauch n-butane, J. Chem. Phys. **73**, 2599-2602 (1980).

9.26 R. Mendelsohn, R.G. Snyder: Infrared spectroscopic determination of conformational disorder and microphase separation in phospholipid acyl chains, in *Biological membranes: A molecular perspective from computation and experiment*, ed. By K.M. Merz & B. Roux (Birkhauser, Boston 1996) pp. 145-174.

9.27 K. Tu, D.J. Tobias, M.L. Klein: Constant pressure and temperature molecular dynamics simulations of crystals of the lecithin fragments: glycerylphosphororylcholine and dilauroylglycerol, J. Phys. Chem. **99**, 10035-10042 (1995).

9.28 D.J. Tobias, K. Tu, M.L. Klein: Assessment of all-atom potentials for modeling membranes: molecular dynamics simulations of solid and liquid alkanes and crystals of phospholipid fragments, J. Chem. Phys. **94**, 1482-1502 (1997).

9.29 H.J.C. Berendsen, B. Egberts, S.J. Marrink, P. Ahlstrom: Molecular dynamics simulations of phospholipid membranes and their interaction with phospholipase A2, in *Membrane proteins: Structures, interactions and models*, ed, by A. Pullman, J. Fortner, B. Pullman (Kluwer Academic Publishers, Amsterdam 1992) pp. 457-470.

9.30 S.E. Feller, D. Yin, R.W. Pastor, A.D. MacKerrell: Molecular dynamics simulation of unsaturated lipid bilayers at low hydration: parameterization and comparison with diffraction studies, Biophys. J. **73**, 2269-2279 (1997).

9.31 S.E. Feller, R.W. Pastor, A. Rojnuckarin, S. Bogusz, B.R. Brooks: Effect of electrostatic force truncation on interfacial and transport properties of water, J. Phys. Chem, **100**, 17011-17020 (1996).

9.32 P.J. Steinbach, B.R. Brooks: New spherical-cutoff methods for long-range forces in macromolecular simulation, J. Comp. Chem. **15**, 667-683 (1994).
9.33 L. Verlet: Computer experiments on classical fluids. I. Thermodynamical properties of Lennard-Jones molecules. Phys. Rev. **159**. 98-103 (1967).
9.34 H.C. Andersen: Molecular dynamics simulations at constant temperature and/or pressure, J. Chem. Phys. **72**, 2384-2393 (1980).
9.35 S. Nose, M.L. Klein: Constant pressure molecular dynamics for molecular systems, Mol. Phys. 50, 1055-1076 (1983).
9.36 W.G. Hoover: Canonical dynamics: Equillibrium phase-space distributions, *Phys. Rev. A* **31**, 1695-1697 (1985).
9.37 S.E. Feller, Y. Zhang, R.W. Pastor, B.R. Brooks: Constant pressure molecular dynamics simulation: The Langevin piston method, J. Chem. Phys. **103**, 4613-4621 (1995).
9.38 S.H. White: Small phospholipid vesicles: internal pressure, surface tension, and surface free energy, Proc. Natl. Acad. Sci. USA **77**, 4048-4050 (1980).
9.39 K. Tu, D.J. Tobias, J.K. Blasie, M.L. Klein: Molecular dynamicds investigation of the structure of a fully hydrated gel phase DPPC bilayer, Biophys. J. **70**, 595-608 (1996).
9.40 F. Jahnig: What is the surface tension of a lipid bilayer membrane?, Biophys. J. **71**, 1348-1349 (1996).
9.41 S.W. Chiu, M. Clark, V. Balaji, H.L. Scott, E. Jakobssen: Incorporation of surface tension into molecular dynamics simulation of an interface: A fluid phase lipid bilayer membrane, Biophys. J. **69**, 1230-1245 (1995).
9.42 S.E. Feller, R.W. Pastor: On simulation lipid bilayers with an applied surface tension: Periodic boundary conditions and undulations, *Biophys. J.* **71**, 1350-1355 (1996).
9.43 S.E. Feller, R.W. Pastor: Length scales of lipid dynamics and molecular dynamics, in *Proceedings of the Pacific Symposium on Biocomputing*, ed. by R.B. Altman, A.K. Dunker, L. Hunter and T.E. Klein (World Scientific, Singapore 1997), pp. 142-150.
9.44 D. Marsh: Renormalization of the tension and area expansion modulus in fluid membranes, Biophys. J. **73**, 865-869 (1997).
9.45 R.W. Pastor, S.E. Feller: Time scales of lipid dynamics and molecular dynamics, in *Biological membranes: A molecular perspective from computation and experiment*, ed. By K.M. Merz & B. Roux (Birkhauser, Boston 1996) pp. 3-30.
9.46 J.F. Nagle, D.A. Wilkinson: Lecithin bilayers: density measurements and molecular interactions, Biophys. J. **23** 159-175 (1978).
9.47 S.H. White, R.E. Jacobs, G.I. King: Partial specific volumes of lipid and water in mixtures of egg lecithin and water, Biophys. J. **52**, 663-665 (1987).
9.48 H.I. Petrache, S.E. Feller, J.F. Nagle: Determination of component volumes of lipid bilayers from simulation, Biophys. J. **72**, 2237-2242 (1997).
9.49 M.C. Wiener, S.H. White: Structure of a fluid dioleoylphosphatidylcholine bilayer determined by joint refinement of x-ray and neutron diffraction data. III. Complete structure, Biophys. J. **61**, 434-447 (1992).
9.50 S.E. Feller, R.M. Venable, R.W. Pastor: Computer simulation of a DPPC phospholipid bilayer: Structural changes as a function of molecular surface area, Langmuir **13**, 6555-6561 (1997).

9.51 W.J. Sun, R.M. Suter, M.A. Knewtson, C.R. Worthington, S. Tristram-Nagle, R. Zhang, J.F. Nagle: Order and disorder in fully hydrated unoriented bilayers of gel phase DPPC, Phys. Rev. E. **49**, 4665-4676 (1994).

9.52 D.M. Small: Phase equilibria and structure of dry and hydrated egg lecithin, J. Lipid. Res. **8**, 551-557 (1967).